Supplementary Information for

Ultrasmall Nanoparticles with Strong Interfacial Interactions for Enhanced Acidic Oxygen Evolution Reaction

Ming Wei[a,b], Liuhua Mu[b,c], Zhiwei Liu [b], Feng Gao[b], Guangjian Song[a,b], Qiankang Si[b] ,Mao Zhang[a], Fangfang Dai[b], Min Zhang[b], Rui Ding[b], Li Yang[a], Zhonggui Gao*[a], Sanzhao Song*[b]*

[a] College of Physics and Technology, Guangxi Normal University, Guilin, 541004, China

[b] Wenzhou Institute, University of Chinese Academy of Sciences, Wenzhou, Zhejiang 325001, China

[c] School of Physical Science, University of Chinese Academy of Sciences, Beijing 100049, China

*Corresponding Author.

E-mail: songsanzhao@ucas.ac.cn (S. S.);
Email: gaozhg3@mailbox.gxnu.edu.cn (Z. G.);
Email: yangli@mailbox.gxnu.edu.cn (L. Y.);

Supporting Experimental Section

Chemicals

Iron chloride ($FeCl_3$, ≥99.99%, Aladdin), Ruthenium (III) chloride hydrate ($RuCl_3 \cdot H_2O$, ≥99.99%, Macklin), Cobalt chloride hexahydrate ($CoCl_2 \cdot 6H_2O$, ≥99.99%, Aladdin), Nafion solution (~5 wt% in a mixture of lower aliphatic alcohols and water, Aldrich), sulfuric acid (H_2SO_4, 95.0%~98.0%). All chemicals were used without further purification directly after purchase. Ultrapure water (18.25 MΩ·cm) produced by the purification system (Ulupure, Sichuan of China) was used for all solutions prepared in the experiments.

Physicochemical characterizations

X-ray diffraction (XRD)

The crystal structures of the synthesized catalysts were analyzed using X-ray diffraction (XRD). The diffraction patterns were obtained with a Bruker D8 Advance X-ray diffractometer (Germany), utilizing nickel-filtered Cu Kα radiation (λ = 1.54178 Å). The scanning parameters were set with a 2θ range of 10-80°, a step size of 0.02°, and the instrument was operated at 40 kV and 40 mA.

Raman measurements

Raman spectra were recorded using an in Via Raman microscope (Renishaw) equipped with a 633 nm excitation laser. The acquisition time for each scan was set to 10 seconds, with a spectral range of 100-1000 cm^{-1}, and the laser power was maintained at 10%.

Scanning electron microscopy (SEM)

Scanning electron microscopy (SEM) was acquired on a SU8010 (Hitachi) with an accelerating voltage of 10 kV and a current of 10 μA. An ethanol dispersion of catalysts was dripped onto the silicon wafer and dried naturally before being used for SEM measurements.

Transmission electron microscopy (TEM)

Transmission electron microscopy (TEM) was acquired on a Talos F200S (Thermo Fisher Scientific) with an accelerating voltage of 200 kV. An ethanol dispersion of catalysts was dripped onto a carbon-coated bicopper grid and then dried naturally for TEM measurements.

N_2 Adsorption-Desorption Isotherm and BET Analysis

The specific surface area of the catalysts was determined using a McMurray Tick surface characterization analyzer (3 Flex) via nitrogen (N_2) adsorption-desorption isotherms. Measurements were conducted at 77.3 K, with N_2 as the adsorbate. The samples underwent pretreatment at 50 °C for 8 hours prior to analysis.

X-ray photoelectron spectra (XPS)

XPS measurements were performed using an ESCALAB Xi+ spectrometer (Thermo Fischer). The instrument utilized a monochromatic Al Kα X-ray source with an energy of 1486.6 eV, operating at a voltage of 12.5 kV and a filament current of 16 mA. The survey spectrum was collected with a pass energy of 100 eV, while the high-resolution spectrum was recorded with a pass energy of 20 eV. The base pressure in the analysis chamber was maintained at 8×10^{-10} mbar during measurements. All binding energies were referenced to the C 1s peak at 284.8 eV.

Electrochemical measurements of OER activities

All electrochemical measurements were conducted using a CHI 760E electrochemical analyzer (Chenhua, Shanghai) at room temperature. A standard three-electrode setup was used, with carbon paper as the working electrode (WE). The catalyst ink was prepared by dispersing 5 mg of electrocatalyst in 200 μL deionized water, 250 μL ethanol, and 50 μL of 5 wt% Nafion solution, followed by sonication for 60 minutes. A 100 μL aliquot of the ink was drop-cast onto a 1 cm × 1 cm carbon paper substrate (Toray Industries, Japan) and allowed to dry naturally. A saturated calomel electrode

(SCE) and a graphite rod were used as the reference electrode (RE) and counter electrode (CE), respectively. All potentials were referenced to the reversible hydrogen electrode (RHE) using the equation:

$$E\ (vs.\ RHE) = E\ (vs.\ SCE) + 0.0591 \times pH + 0.24\ V$$

The electrolyte used was 0.5 M H_2SO_4 (80 mL). The catalyst was fully activated using cyclic voltammetry (CV) before measurements. Polarization data were collected using linear sweep voltammetry (LSV) at a scan rate of 5 $mV \cdot s^{-1}$.

Electrochemical impedance spectroscopy (EIS) was performed in the frequency range of 0.1 Hz to 100 kHz with an AC amplitude of 10 mV. The electrochemical active surface area (ECSA) was determined using the CV method, with CV curves recorded at scan rates of 20, 40, 60, 80, 100, and 120 $mV \cdot s^{-1}$ within the potential range of 1.06 to 1.16 V vs. RHE, where no Faradaic processes occur. The scan rate was plotted as the horizontal axis and half of the difference between the positive and negative current densities at the center of the scanning potential range (i.e., 1.11 V vs. RHE of the OER) was plotted as the vertical axis, with the slope representing the double-layer capacitance (C_{dl}).

Stability tests were conducted using the galvanostatic method at a current density of 10 $mA \cdot cm^{-2}$.

The mass activity (MA) was calculated using the equation:

$$Mass\ Activity = j / m.$$

where j is the current density ($mA \cdot cm^{-2}$) measured at 1.60 V vs. RHE, and m is the catalyst loading (1 $mg \cdot cm^{-2}$).

For overall water splitting, the RFC catalyst was used as the anode in a two-electrode system with a proton exchange membrane (PEM) and commercial 20% Pt/C as the cathode. The electrolyte was 0.5 M H_2SO_4. The catalyst was activated using CV before measurements. LSV was performed at a scan rate of 5 $mV \cdot s^{-1}$, and stability tests were conducted using the galvanostatic method at a current density of 10 $mA \cdot cm^{-2}$.

Supporting Figures.

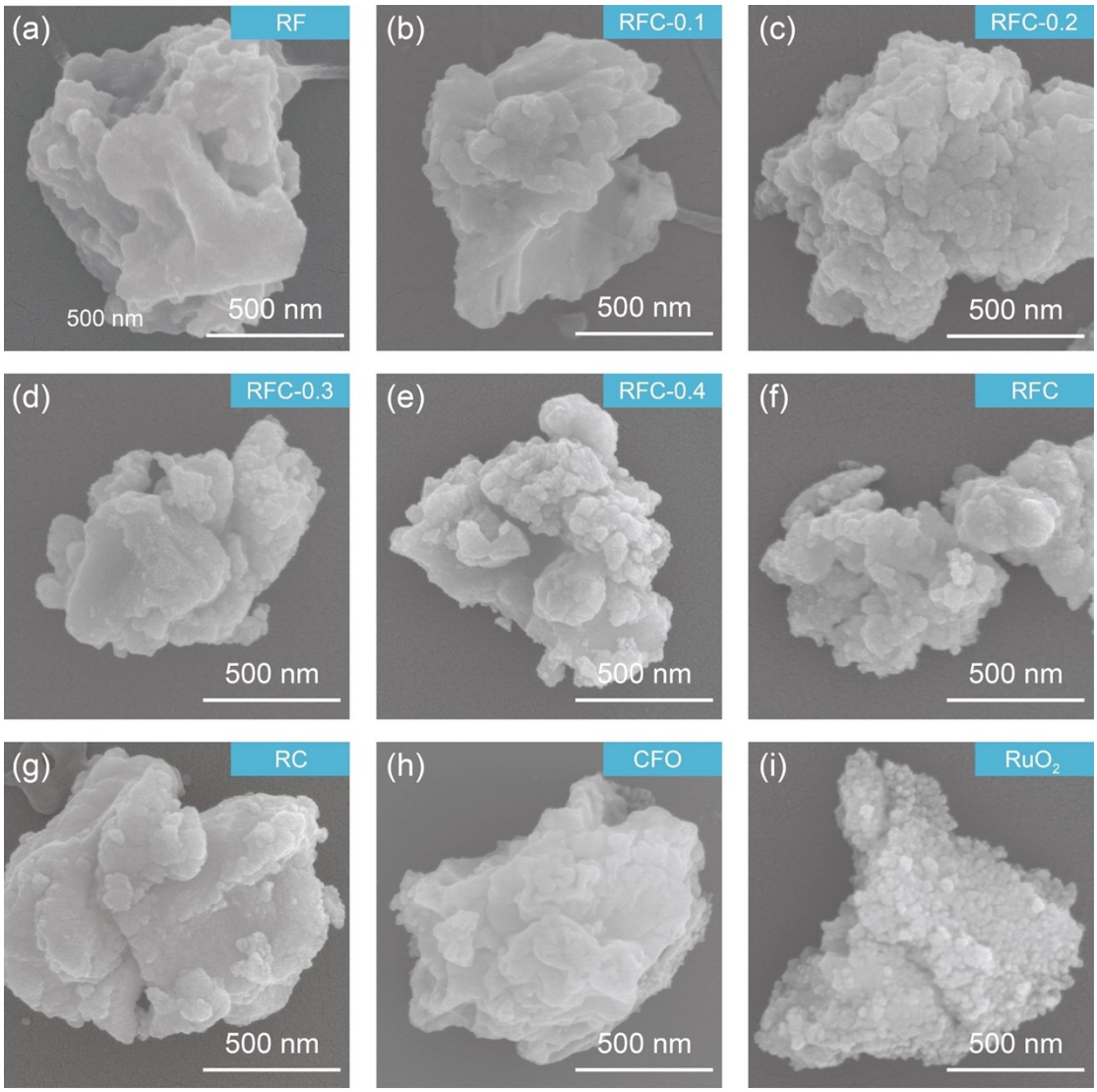

Fig. S1. SEM images of catalysts.

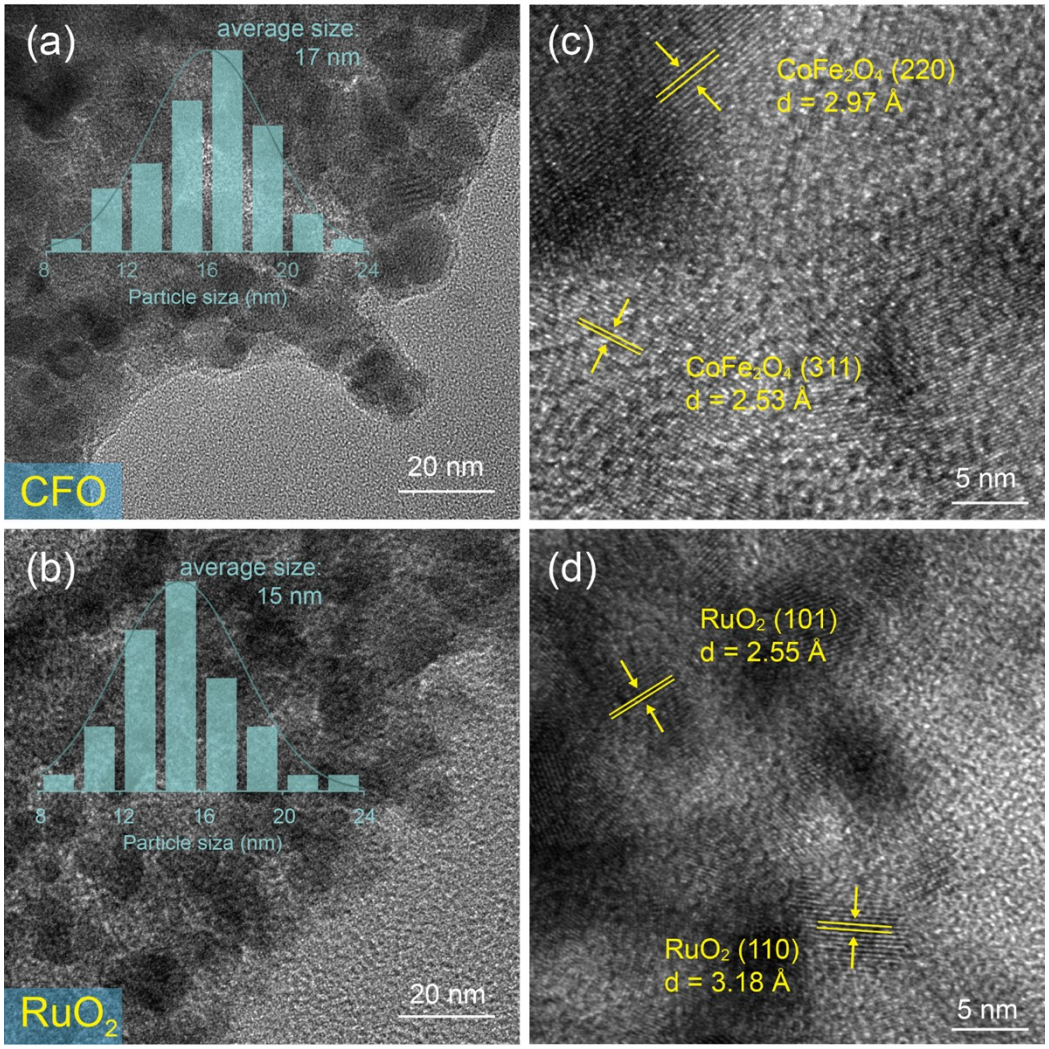

Fig. S2. TEM images of (a) CFO and (b) RuO_2. HRTEM images of (c) CFO and (d) RuO_2.

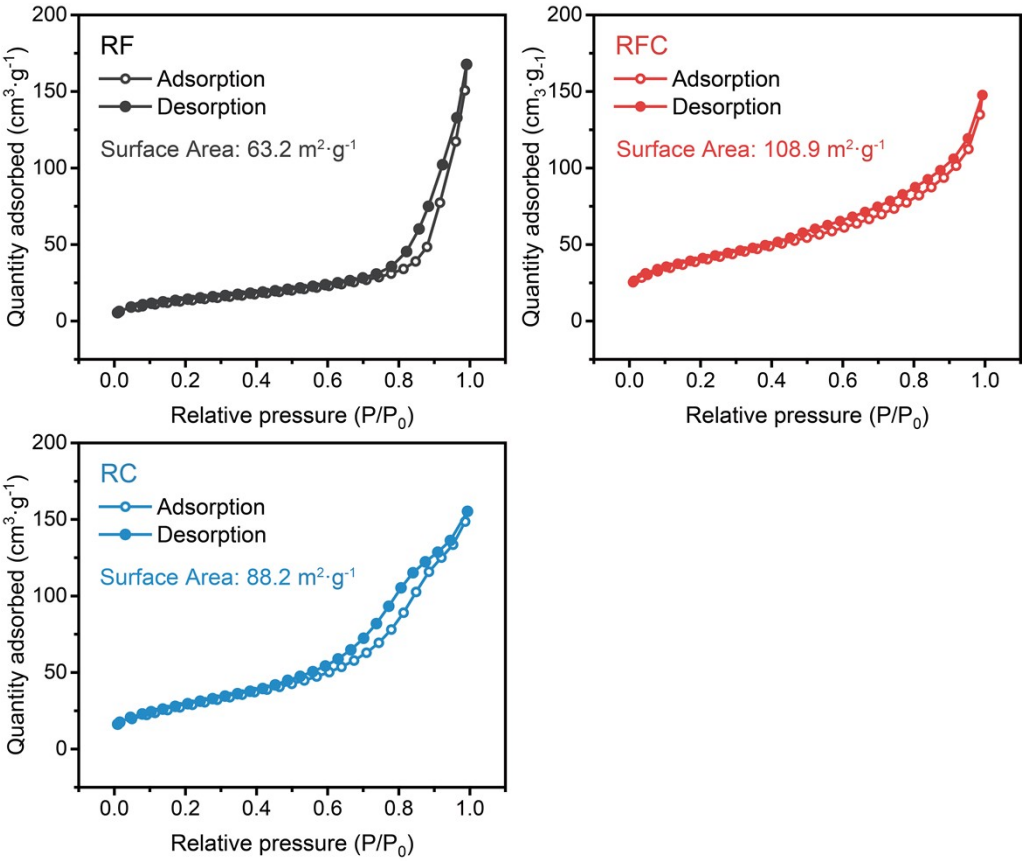

Fig. S3. Nitrogen Adsorption-desorption isotherm curve of catalysts.

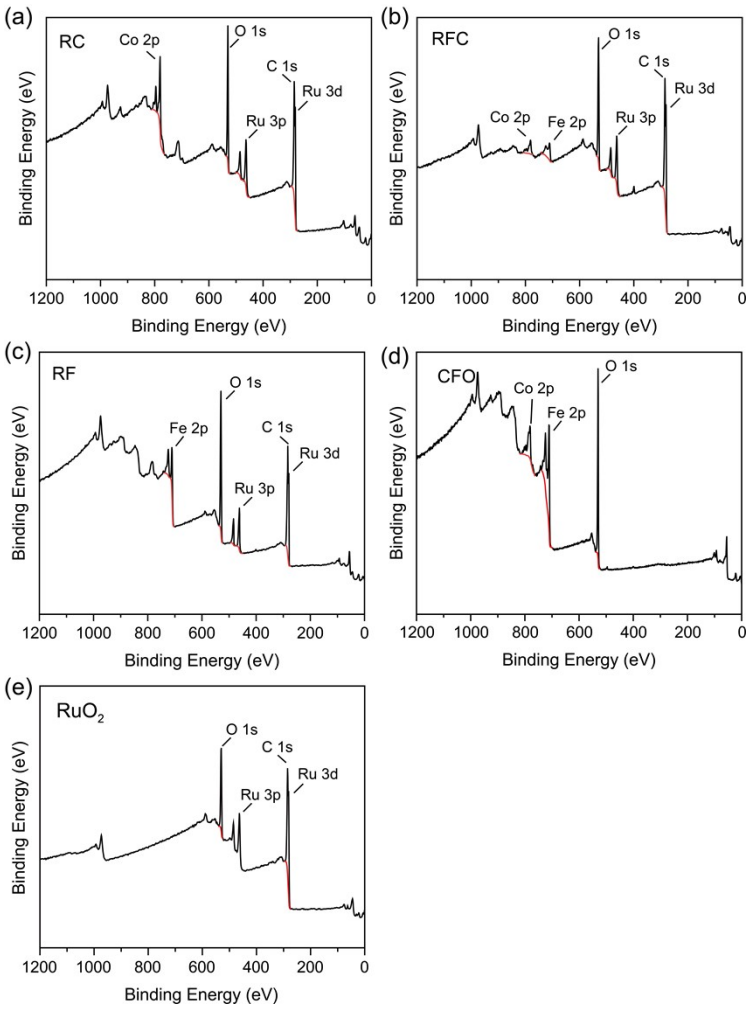

Fig. S4. XPS survey spectra of catalysts.

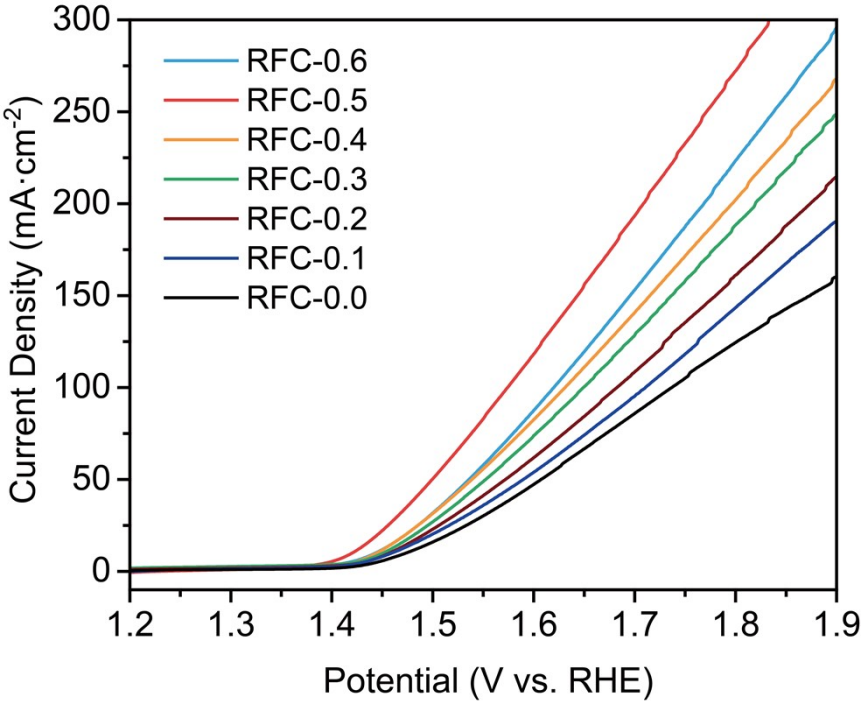

Fig. S5. LSV curves of RFC catalysts with different concentrations of Co^{2+}.

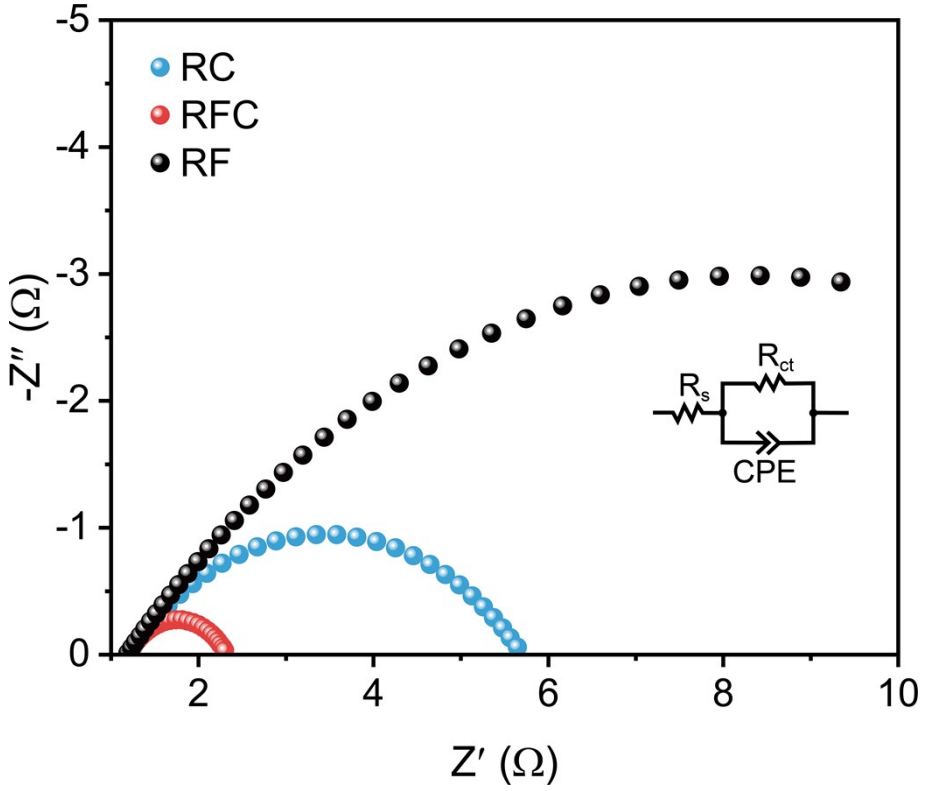

Fig. S6. EIS Nyquist plots of catalysts at a potential of 1.40 V (vs. RHE).

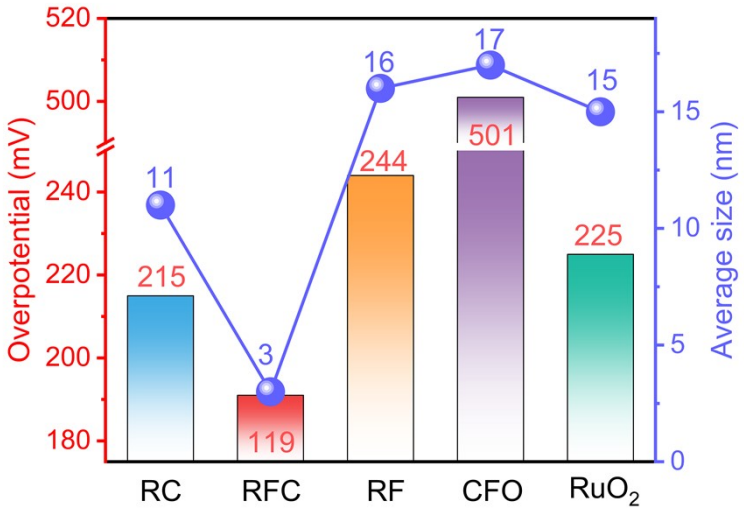

Fig. S7. Comparison of the overpotentials at 10 mA cm^{-2} and average particle sizes for different catalysts.

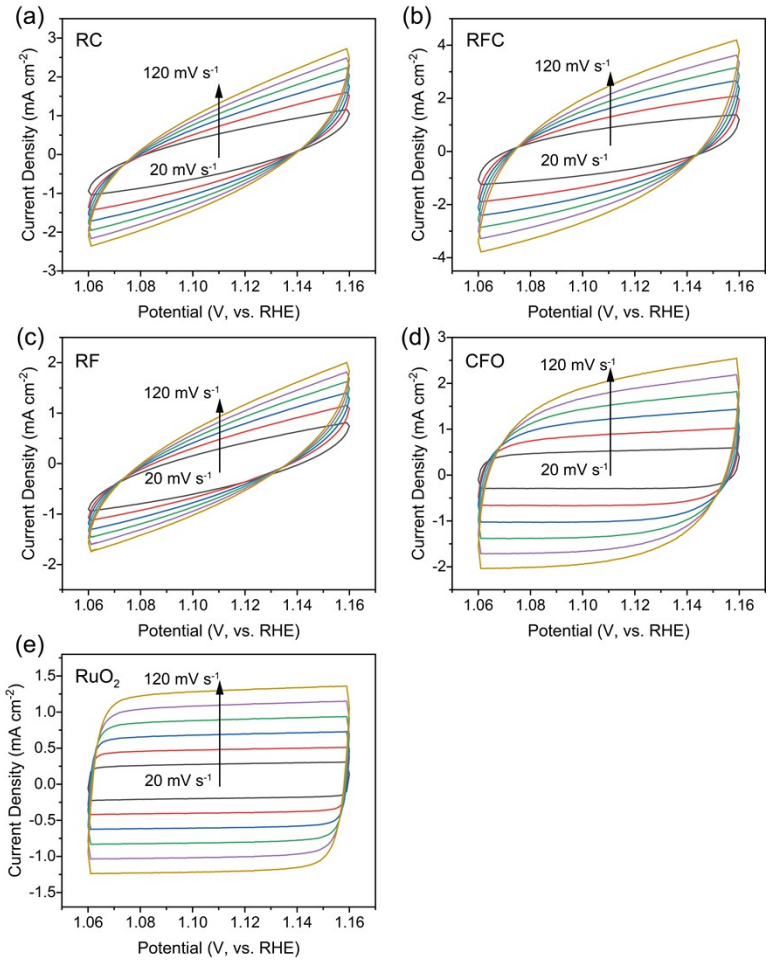

Fig. S8. Electrochemical active surface area (ECSA) analyses of catalysts according to the CV at different sweep speed of in a potential window (1.06~1.16 V vs. RHE) where no Faradaic processes occur for catalysts.

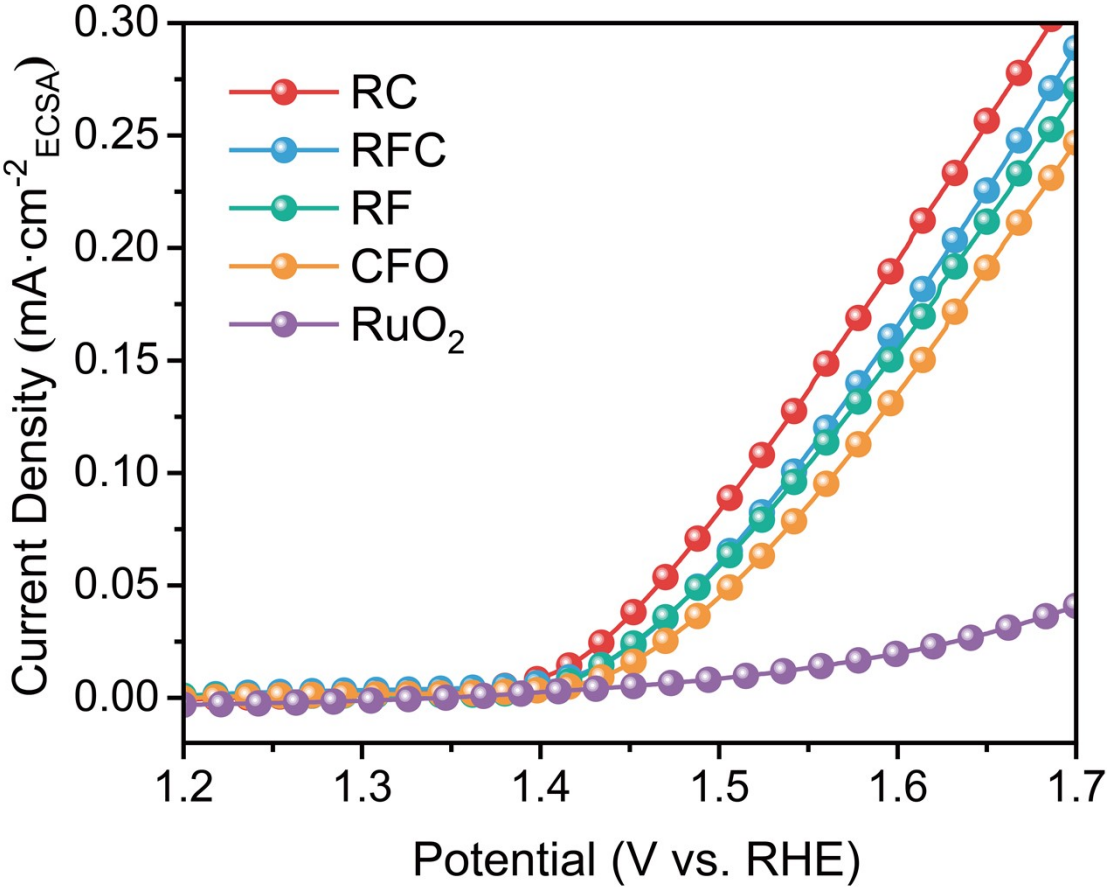

Fig. S9. Linear sweep voltammetry (LSV) curves normalized to ECSA for the oxygen evolution reaction (OER) in 0.5 M H_2SO_4.

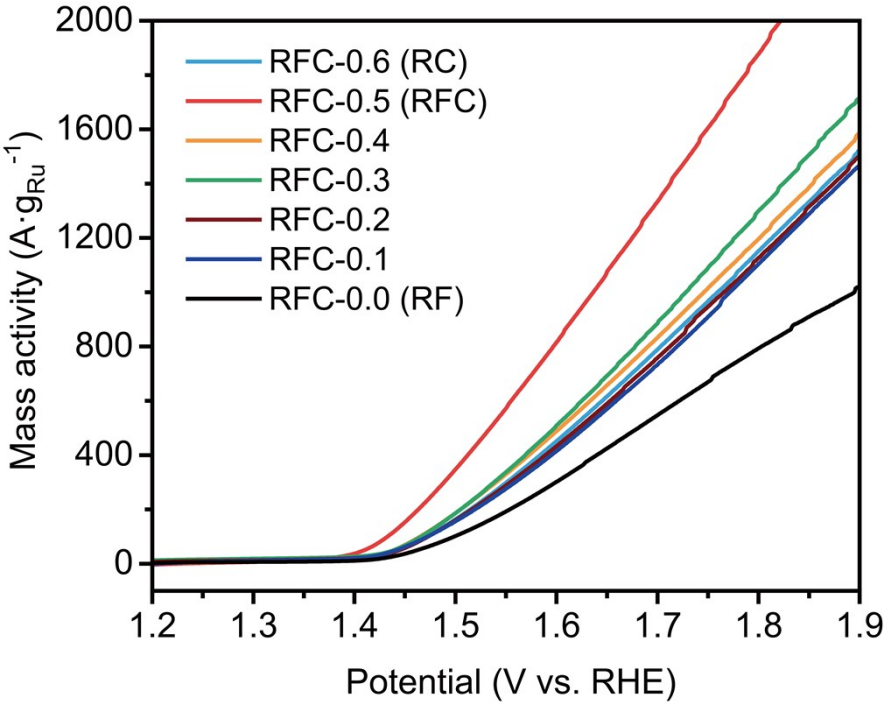

Fig. S10. Mass Activity-Normalized Linear Sweep Voltammetry (LSV) Curves.

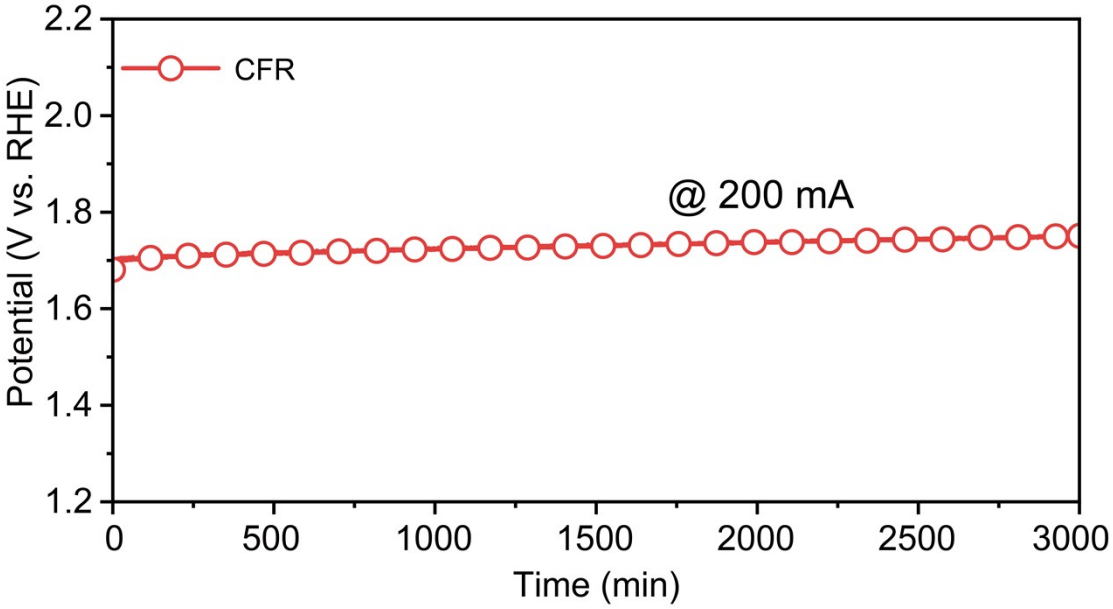

Fig. S11. Stability test of catalysts at 200 mA cm^{-2}.

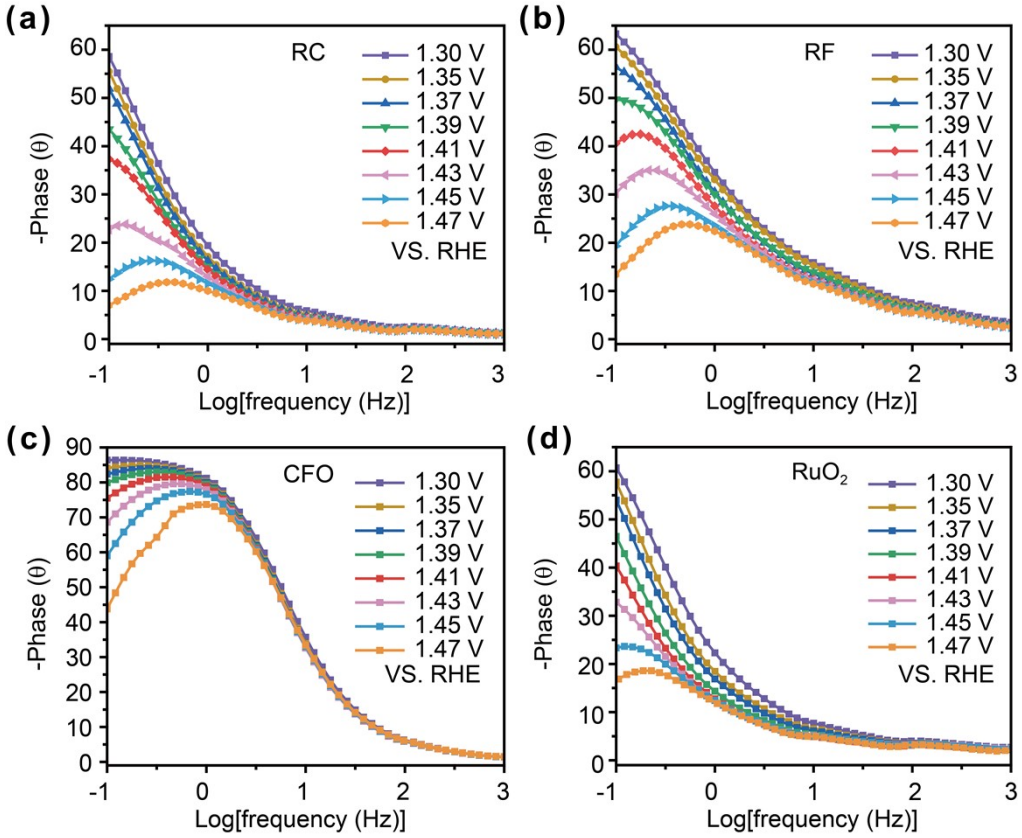

Fig. S12. Bode phase plots of (a) RC, (b) RF, (c) CFO and (d) RuO_2

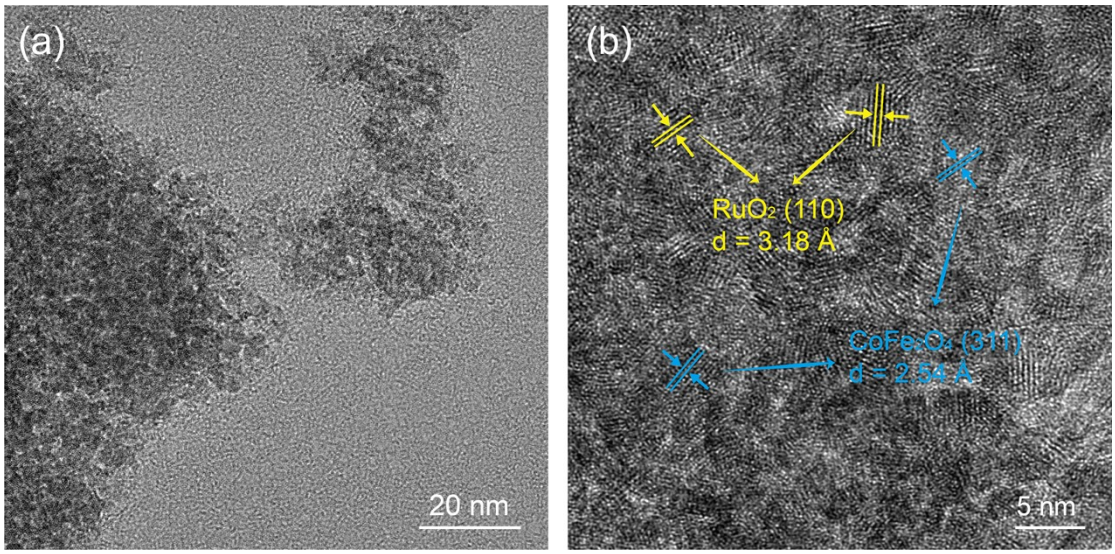

Fig. S13. TEM images of RFC catalyst after stability test.

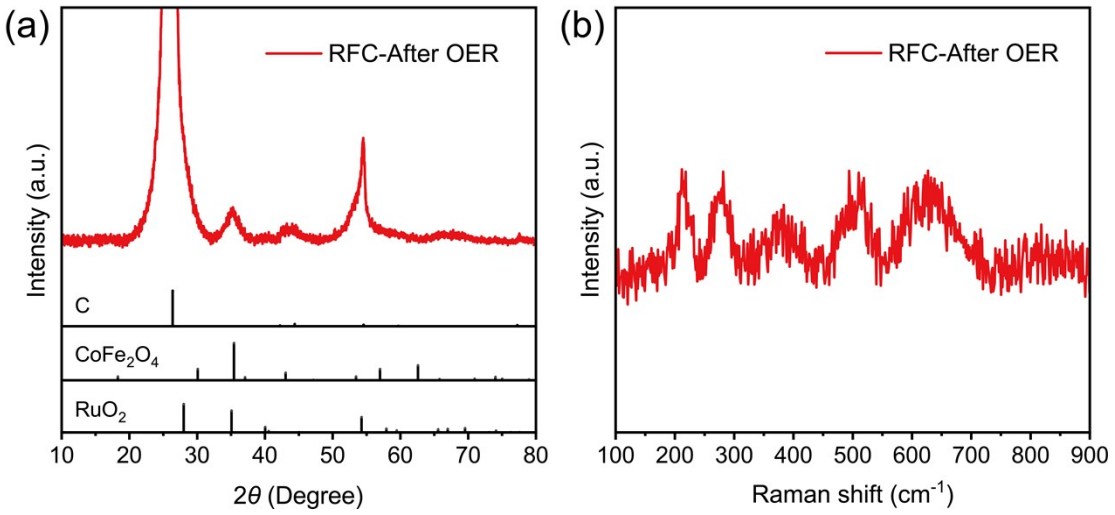

Fig. S14 (a) XRD spectra and (b) Raman spectra of the RFC catalyst after stability test.

Supporting Tables

Table S1. Name of catalyst and ion concentration of precursor during preparation.

C	Co^{2+} (ppm)	Fe^{3+} (ppm)	Ru^{3+} (ppm)
RFC-0.0 **(RF)**	0	600	300
RFC-0.1	100	500	300
RFC-0.2	200	400	300
RFC-0.3	300	300	300
RFC-0.4	400	200	300
RFC-0.5 **(RFC)**	500	100	300
RFC-0.6 **(RC)**	600	0	300

Table S2. Elemental composition in weight percentages (wt%) as measured by ICP-MS.

Sample	**Co (**wt **%)**	**Ru (** wt **%)**	**Fe (** wt **%)**
RFC-0.0 **(RF)**	0.0	15.7	85.3
RFC-0.1	7.8	12.3	79.9
RFC-0.2	10.6	14.1	75.3
RFC-0.3	15.3	15.8	68.9
RFC-0.4	19.7	17.6	62.7
RFC-0.5 **(RFC)**	28.2	14.5	57.3
RFC-0.6 **(RC)**	80.6	19.4	0.0

Table S3: Elemental composition in Atomic Percentages (at%) as measured by ICP-MS.

Sample	**Co (**at **%)**	**Ru (**at **%)**	**Fe (**at **%)**
RFC-0.0 **(RF)**	0.0	25.0	75.0
RFC-0.1	7.5	20.1	72.4
RFC-0.2	10.0	22.8	67.2
RFC-0.3	14.2	25.2	60.6
RFC-0.4	18.0	27.6	54.4
RFC-0.5 **(RFC)**	26.3	23.2	50.6
RFC-0.6 **(RC)**	70.8	29.2	0.0

Table S4. Different oxygen content in the catalyst.

Samples	O_1 (%)	O_2 (%)	O_3 (%)
RC	55	30	15
RFC	36	45	19
RF	47	41	12
CFO	66	19	14
RuO_2	41	43	16

Table S5. Ruthenium (Ru) Load on 1 cm² Carbon Paper Electrodes for Different Catalyst Samples

Sample	Ru Load (mg)
RFC-0.0 **(RF)**	0.157
RFC-0.1	0.123
RFC-0.2	0.141
RFC-0.3	0.158
RFC-0.4	0.176
RFC-0.5 **(RFC)**	0.145
RFC-0.6 **(RC)**	0.194

Table S6. Comparative evaluation of recently reported Ru-based electrocatalysts in acidic media.

Catalyst	Overpotential (mV) @10mA cm^{-2}	Stability @10 mA cm^{-2}	Ref.
Fe_2O_3@RuO_2	191	100 h 3000 min @200 mA cm^{-2}	**This work**
C-RuO_2-RuSe	212	50	Chem 2022, 8, 1673-1687
RuO_2-WC NPs	347	10	Angew. Chem. Int. Ed. 2022, 61, e20220251911
Na-a/c-RuO_2	205	60	Angew. Chem. Int. Ed. 2021, 60, 18821-18829
Ru/RuS_2	201	24	Angew. Chem. Int. Ed. 2021, 60, 12328-1233423
$Y_{1.7}Sr_{0.3}Ru_2O_7$	264	28	ACS Nano 2021, 15, 8537-8548
RuIr@CoNC	223	40	ACS Catal. 2021, 11, 3402-3413
$CaCu_3Ru_4O_{12}$	273	59	Small 2022, 18, 2202439
RuO_2 nanowires	224	12	Adv. Funct. Mater. 2021, 31, 2007344
Zn-doped RuO_2	206	30	ChemNanoMat 2021, 7, 117-121
Ru@IrOx	282	24	Chem 2019, 5, 445
B-RuO_2	200	40	Nano Res. 2022, 15, 7008